

# Arbitrary Time Shaping of Broadband Low-Coherence Light Based on Optical Parametric Amplification

Yue Wang <sup>1,2</sup>, Xiaochao Wang <sup>1,\*</sup>, Meizhi Sun <sup>1</sup>, Xiao Liang <sup>1</sup> , Hui Wei <sup>1</sup> and Wei Fan <sup>1</sup>

<sup>1</sup> Key Laboratory on High Power Laser and Physics, Shanghai Institute of Optics and Fine Mechanics, Chinese Academy of Sciences, Shanghai 201800, China; yuewang@siom.ac.cn (Y.W.)

<sup>2</sup> Center of Materials Science and Optoelectronics Engineering, University of the Chinese Academy of Sciences, Beijing 100049, China

\* Correspondence: smilexc@siom.ac.cn

**Abstract:** Laser–plasma interactions (LPIs) hinder the interaction of high-energy laser pulses with targets. The use of broadband low-coherence light has been proposed to reduce the impact of LPIs. In this study, to improve the time–frequency characteristics of broadband low-coherence optical seeds, we proposed an arbitrary time-shaping technique scheme based on optical parametric amplification (OPA) that differs from traditional arbitrary time shaping. The shaping process and output characteristics were analyzed in detail. The theoretical and experimental results show that an arbitrary time-shaping pulse output with a large time-shaping contrast, fast-rising edge, and wide spectral width can be obtained. The time shaping contrast of the shaped pulse can be >300:1, and the spectral width is ~40 nm. The output time waveform is smoother than in traditional schemes, and the noise-like modulation is approximately 4% (approximately equal to the unshaped initial amplified spontaneous emission source). The arbitrary time-shaping scheme based on OPA provides a viable solution for the temporal waveform shaping of broadband low-coherence light.

**Keywords:** ICF; laser–plasma interaction; broadband low-coherence light source; arbitrary time shaping; OPA



**Citation:** Wang, Y.; Wang, X.; Sun, M.; Liang, X.; Wei, H.; Fan, W. Arbitrary Time Shaping of Broadband Low-Coherence Light Based on Optical Parametric Amplification. *Photonics* **2023**, *10*, 673. <https://doi.org/10.3390/photonics10060673>

Received: 14 April 2023

Revised: 31 May 2023

Accepted: 8 June 2023

Published: 9 June 2023



**Copyright:** © 2023 by the authors. Licensee MDPI, Basel, Switzerland. This article is an open access article distributed under the terms and conditions of the Creative Commons Attribution (CC BY) license (<https://creativecommons.org/licenses/by/4.0/>).

## 1. Introduction

The physical study of inertial confinement fusion (ICF) [1] allows us to observe the parametric and hydrodynamic instability occurring in high-intensity laser–plasma interaction (LPI) [2,3]. This can significantly reduce laser utilization efficiency. LPI is a major factor limiting the success of fusion. To address this problem, scholars have proposed techniques such as smoothing using spectral dispersion, polarization smoothing, continuous phase plates, and the introduction of a magnetic field; however, they still do not satisfy the physical requirements [4–7]. In recent years, several researchers have suggested that the LPI effect can be improved by limiting the nonlinear effects to a lower level using special time–frequency-characterized light sources [8–10]. The currently accepted technical solution is the use of a broadband low-coherence light source. In 2019, Cui et al. proposed a high-energy, low-temporal-coherence transient broadband pulse system with an amplified spectral width of ~10 nm, an output pulse coherence time of 318 fs, and energy up to ~1 kJ [11,12]. In 2020, the University of Rochester reported the high-energy optical parametric amplification of spectrally incoherent signal systems. Signals composed of mutually incoherent monochromatic lines or amplified spontaneous emissions were amplified using a sequence of optical parametric amplifiers pumped at 526.5 nm, with the last amplifier set in a collinear geometry. They achieved an output of up to several hundred millijoules of energy and an incoherent spectrum extending over 60 nm [13].

A high-energy laser driver of ICF is composed of a front end, pre-amplifier, main amplifier, target, and other diagnostic systems. As an injection laser system, a nanosecond laser pulse of the front end should possess certain features, such as an arbitrary time waveform,

high signal-to-noise ratio, and good stability [14]. In the aforementioned study, an amplified spontaneous emission (ASE) in the fiber shaped by an electro-optical modulator was used as the time-shaping front end, and the article mentioned that the arbitrary time-shaping schemes of the traditional front end still encounter problems with the arbitrary time shaping of broadband low-coherence light [13]. Electro-optical modulators are modulators that utilize the electro-optical effect of certain crystals, such as lithium niobate crystals ( $\text{LiNbO}_3$ ). The electro-optical effect is such that when a voltage is applied to an electro-optical crystal, the refractive index of the crystal changes, resulting in a change in the characteristics of the light wave passing through the crystal, modulating the amplitude of the optical signal. It is based on the interference principle, which can lead to the introduction of Fabry–Perot filtering and high-frequency noise-like modulation [15,16] on the time waveform. Research on the time–frequency characteristic change processes of broadband low-coherence optical modulation is not sufficient, particularly the high-frequency noise-like modulation caused by processes such as time shaping. This is a safety threat for high-power laser devices and a problem that must be clarified and addressed. Researchers have made many attempts to address these problems. In 2020, the Shanghai Institute of Optics and Fine Mechanics proposed and experimentally demonstrated a scheme to achieve the all-optical arbitrary temporal shaping of broadband low-coherence light based on a saturable absorption effect. Compared with traditional temporal shaping schemes, such as electro-optic modulation (EOM) shaping or acousto-optic modulation (AOM) shaping, the modulation on the shaped pulse profile is significantly smaller. However, problems still occur, such as low signal-to-noise ratios [17]. In 2022, the University of Rochester proposed a closed-loop control of the spectral density and pulse shape of nanosecond spectrally incoherent pulses after optical parametric amplification in infrared (approximately 1053 nm) and sum-frequency generation to ultraviolet (approximately 351 nm) using spectral and temporal modulation in the front end [18]. They obtained the spectral density and pulse shape of nanosecond spectrally incoherent pulses. However, they did not discuss the characteristics of the time-shaping pulse using optical parametric amplification (OPA) in detail.

Most applications of optical parametric amplifiers are based on the interactions of spectrally coherent waves. However, their operation with spectrally incoherent waves has also been reported. For example, the operation of an optical parametric amplifier with a spectrally incoherent signal was simulated and demonstrated in the context of polychromatic image amplification and the generation of parametric fluorescence pulses at the microjoule level using femtosecond pump pulses [19,20]. The operation of optical parametric amplifiers with spectrally incoherent pump pulses was described in the context of multiplexing different pump sources [21].

In this study, OPA-based time-shaping schemes were used in a broadband low-coherence arbitrary time-shaping approach to address high-frequency modulation. In the OPA-based time-shaping system, the gain in the signal in the coupling process between the pump and the signal is related to the intensity of the pump. The temporal intensity distribution of the signal is determined using the pump intensity distribution. By shaping the pump temporal pulse, we can obtain broadband low-coherence signals of arbitrary shapes. We also discuss the temporal and spectral characteristics of the signal pulse during the shaping process in detail.

## 2. Principle and Scheme

Because the main advantage of a broadband low-coherence light source is its low-coherence spectral characteristics [22–24], we must consider the effect of the time-shaping process on the spectral coherence of the source. This ensures that the low-coherence characteristics of the light source will not decrease or even disappear because of shaping and that the time-domain waveform obtained by shaping is smooth. Currently, the mature time-domain shaping scheme in ICF experiments uses electro-optic modulators for shaping, such as the Mach–Zehnder (M-Z) modulator, whose principles are based on the interference of light. Because the interference effect is wavelength-dependent, for broadband light sources, the time-shaping process causes missing spectra, resulting in the introduction of

high-frequency modulation in the time domain, which cannot guarantee complete time-domain shaping. To address this problem, we propose an arbitrary time-shaping scheme based on OPA and present a detailed time–frequency characterization.

Simulations of the parametric gain in a nonlinear crystal require the propagation of the signal, idler, and pump fields in the presence of linear and nonlinear effects. We followed the approach and notations described by Arisholm [25]. OPA is a frequency-conversion technique based on a second-order nonlinear  $\chi^{(2)}$  process. The high-energy pump (frequency  $\omega_p$ ) is passed to the low-frequency signal (frequency  $\omega_s$ ) and the idler signal (frequency  $\omega_i$ ) through the mutual coupling of the optical waves. When light propagates through a medium, whether linear or nonlinear, it is subject to Maxwell’s equations:

$$\begin{aligned} \nabla \cdot \vec{D} &= \rho \\ \nabla \cdot \vec{B} &= 0 \\ \nabla \times \vec{E} &= -\frac{\partial \vec{B}}{\partial t} \\ \nabla \times \vec{H} &= \vec{j} + \frac{\partial \vec{D}}{\partial t} \end{aligned} \tag{1}$$

For a non-magnetic ideal medium ( $\mu = 1$ ), the corresponding equation of matter can be expressed as:

$$\begin{aligned} \vec{D} &= \epsilon_0 \vec{E} + \vec{P} \\ \vec{B} &= \mu_0 \vec{H} \\ \rho &= 0 \\ \vec{j} &= \sigma \vec{E} = 0 \end{aligned} \tag{2}$$

In a vacuum,  $\epsilon_0$  denotes the dielectric constant,  $\mu_0$  denotes the magnetic permeability, and  $\sigma$  denotes the electrical conductivity; for a theoretical typical dielectric,  $\sigma = 0$ . Performing the  $\nabla \times$  operation on Equation (2) combined with other equations yields the following:

$$\nabla \times \nabla \times \vec{E} + \mu_0 \epsilon_0 \frac{\partial^2 \vec{E}}{\partial t^2} = -\mu_0 \frac{\partial^2 \vec{P}}{\partial t^2} \tag{3}$$

Using the vector operator rule  $\nabla \times \nabla \times \vec{E} = \nabla(\nabla \cdot \vec{E}) - \nabla^2 \vec{E}$  and some approximations to calculate  $\nabla \cdot \vec{E} = 0$ , the following equation can be derived:

$$\nabla^2 \vec{E} - \mu_0 \epsilon_0 \frac{\partial^2 \vec{E}}{\partial t^2} = \mu_0 \frac{\partial^2 \vec{P}}{\partial t^2} \tag{4}$$

Equation (4) can be used to represent the correspondence between the electric field strength of the light wave  $\vec{E}$  and the dielectric polarization strength  $\vec{P}$ , where the dielectric polarization intensity can be divided into two components, denoted as  $\vec{P}^{(1)}$  and  $\vec{P}^{(NL)}$ , for the linear and nonlinear components:

$$\vec{P} = \vec{P}^{(1)} + \vec{P}^{(NL)} \tag{5}$$

where the dielectric constant can be expressed as  $\epsilon^{(1)} = 1 + \chi^{(1)}$ , and Equation (4) can be expressed as:

$$\nabla^2 \vec{E} - \mu_0 \epsilon_0 \epsilon^{(1)} \frac{\partial^2 \vec{E}}{\partial t^2} = \mu_0 \frac{\partial^2 \vec{P}^{(NL)}}{\partial t^2} \tag{6}$$

The dielectric constant  $\vec{\epsilon}$  is a parameter that describes the electrical properties of a medium. In anisotropic media, the electric displacement  $\vec{D}$  and the electric field intensity  $\vec{E}$  satisfy the following relationship:

$$\vec{D} = \vec{\epsilon} \cdot \vec{E} = \epsilon_0 \vec{\epsilon}^{(1)} \cdot \vec{E} \tag{7}$$

The electric field distributions of three narrow-linewidth plane waves with frequencies  $\omega_p, \omega_s, \omega_i$  can be expressed as:

$$\begin{aligned} \vec{E}_s(\vec{r}, t) &= \vec{e}_s A_s e^{-j(\omega_s t - \vec{k}_s \cdot \vec{r})} \\ \vec{E}_i(\vec{r}, t) &= \vec{e}_i A_i e^{-j(\omega_i t - \vec{k}_i \cdot \vec{r})} \\ \vec{E}_p(\vec{r}, t) &= \vec{e}_p A_p e^{-j(\omega_p t - \vec{k}_p \cdot \vec{r})} \end{aligned} \tag{8}$$

$$\vec{k}_s = \vec{k}_s(\omega_0) + \delta \vec{k}_s(\omega) \tag{9}$$

Without considering absorption, Equation (6) can be rewritten as:

$$\nabla \times \nabla \times \vec{E} + \mu_0 \epsilon_0 \frac{\partial^2}{\partial t^2} (\vec{\epsilon}^{(1)} \cdot \vec{E}) = -\mu_0 \frac{\partial^2 \vec{P}_{NL}}{\partial t^2} \tag{10}$$

It satisfies the energy conservation condition ( $\omega_p = \omega_s + \omega_i$ ) between frequencies. To attain high conversion efficiency, we select a suitable nonlinear crystal and direction ( $\Delta \vec{k} = \vec{k}_p - \vec{k}_s - \vec{k}_i = 0$ ) to satisfy the phase-matching condition. The wave vectors of the pump, signal, and idle light are  $\vec{k}_p, \vec{k}_s,$  and  $\vec{k}_i,$  respectively. The angles between the pump and the signal and the idle are  $\rho_s$  and  $\rho_i.$  Under the slow-varying envelope approximation, the group velocity mismatch problem and the diffraction can be completely ignored considering that the pulse width of the acting optical wave is in the nanosecond range. The coupled wave equation of the OPA is:

$$\begin{aligned} \frac{\partial A_s}{\partial z} + \tan \rho_s \frac{\partial A_s}{\partial y} &= -j \frac{\omega_s d_{eff}}{c n_s \cos \rho_s} A_i^* A_p e^{-j \Delta k z} \\ \frac{\partial A_i}{\partial z} + \tan \rho_i(t) \frac{\partial A_i}{\partial y} &= -j \frac{\omega_i d_{eff}}{c n_i \cos \rho_i} A_s^* A_p e^{-j \Delta k z} \\ \frac{\partial A_p}{\partial z} + \eta \tan \rho_p \frac{\partial A_p}{\partial y} &= -j \frac{\omega_p d_{eff}}{c n_p} A_s A_i e^{j \Delta k z} \end{aligned} \tag{11}$$

where  $d_{eff}$  is the effective nonlinear coefficient, and  $\Delta \vec{k} = \vec{k}_p - \vec{k}_s - \vec{k}_i$  is the wave-vector mismatch at the center frequencies [13]. The following parameters represent spatial walk-off in crystals:

$$\begin{aligned} \eta &= \frac{n_{pY}^2 n_{pX}^2}{n_{pZ}^2 n_p^2} \\ \tan \rho_p &= \frac{1}{2} n_p^2 \sin 2\alpha \left( \frac{1}{n_{pX}^2} - \frac{1}{n_{pY}^2} \right) \end{aligned} \tag{12}$$

The coupled-wave equations for the OPA can be solved numerically using a stepwise Fourier algorithm [26], including linear frequency-domain and nonlinear time-domain calculations with Fourier and inverse Fourier transforms at each step. In a linear process, for a given step  $\delta z,$  the signal, idle, and pump responses are  $\delta k_s(\omega) \delta z, \delta k_i(\omega) \delta z,$  and  $\delta k_p(\omega) \delta z,$  respectively. For nonlinear processes, the fourth-order Runge-Kutta method is used to calculate parametric amplification.

Our arbitrary shaping system scheme improves the effect of conventional shaping on broadband light as shown in Figure 1. In our scheme, the time shaping is realized in an OPA process. The pump light of the OPA is a narrowband light with an arbitrary time-shaping capability. The signal light of the OPA is a time-continuous broadband low-coherence seed source. The OPA process uses an LBO crystal to ensure that the pump and signal are

incident at a phase-matched angle. The gain of the coupling process between the pump and the signal is related to the intensity of the pump. As the pump power varies with time, based on the OPA principle, the gain in the signal light also changes accordingly. The intensity distribution of the pump determines the signal intensity distribution and, therefore, indirectly shapes the temporal characteristics of the signal. By adjusting the time waveform of the pump light, the ability to control the time waveform of the signal light is obtained.

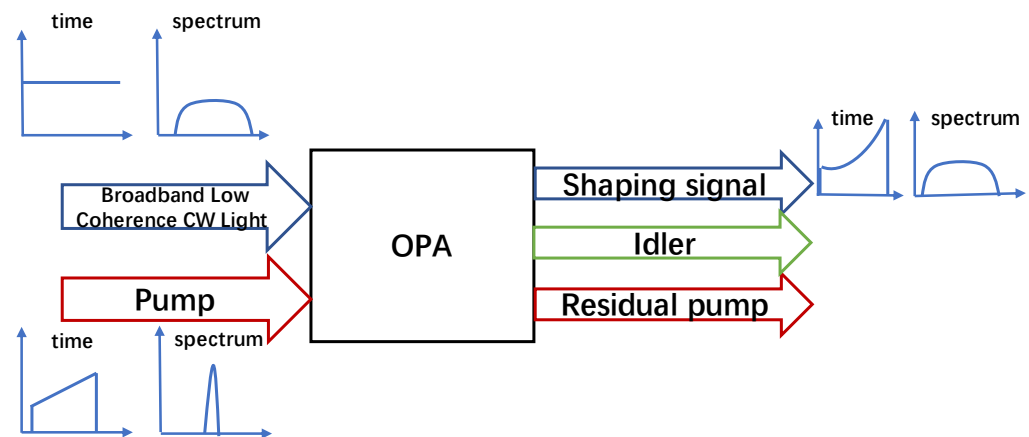


**Figure 1.** OPA-based time shaping structure. The broadband spectral continuous signal is incident with a narrowband shaping pump to produce a broadband-shaped output signal.

### 3. Simulations and Experimental Results

#### 3.1. Simulations Results

With the slow-varying envelope approximation and group velocity mismatch problem being negligible, we calculated the OPA simulation model presented above using a stepwise Fourier algorithm. Because the injected seed source is a broadband low-coherence ASE whose spectrum is narrower than the matched bandwidth, the effect of phase mismatch on the spectrum can be neglected. We simulated a 532 nm pump and a 1053 nm broadband low-coherence signal incident at a phase-matched angle to an LBO crystal with a length of 5 cm. The pump intensity was  $1 \text{ GW/cm}^2$  and the pulse width was 2 ns. The signal was continuous and the signal power was 10 mW. The shaping capability, signal-to-noise ratio, rising edge, and spectral characteristics of an arbitrary time-shaping process were investigated.

In most nanosecond laser pulse-driven ICFs, the time shaping of the seed source requires the output of pulses with a certain time–waveform contrast considering the necessity for gain saturation in subsequent systems and the target compression process in physical experiments [14]. The time-shaping contrast is defined as the intensity ratio between the highest and the lowest power of the shaped time waveform, which is typically in the order of several hundred to one [14]. We simulated the shaping of signal pulses by modulating the pump under various time-shaping contrast conditions as shown in Figure 2. When the time-shaping contrast of the pump is 2:1, the time-shaping contrast of the output shaped signal is 3:1 while the time-shaping contrast of the pump is 100:1, and the contrast ratio of the output pump is 400:1. We observed that the shaped output pulse responded to the shape and time waveform contrast of the pump. An output signal with an arbitrary waveform was obtained by modulating the pump. It shows that the scheme can be used to obtain high time-shaping contrast signal light and can obtain amplified output pulses with flexible time-shaping contrast, which can be applied to a wide range of high-power laser experiments.

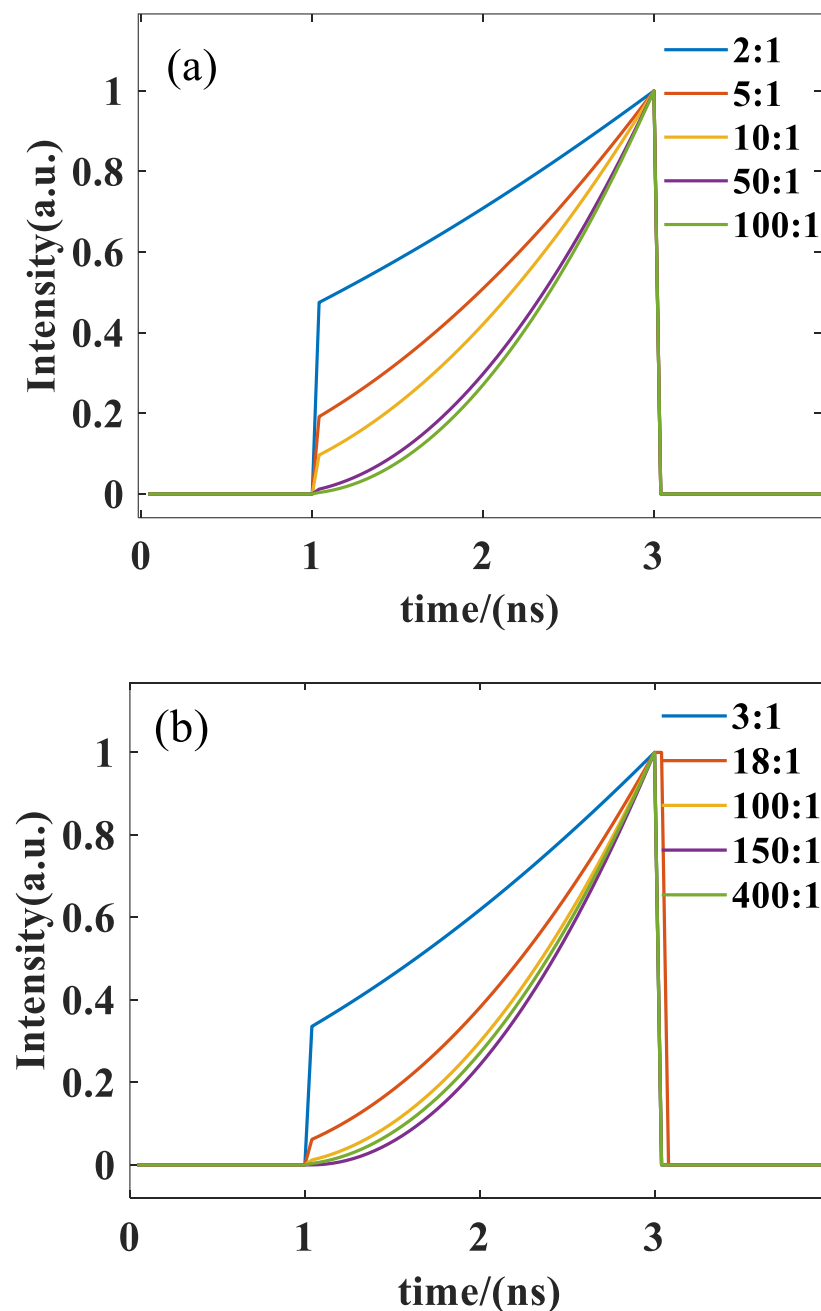


**Figure 2.** Simulation results of the temporal waveforms of (a) pump and (b) shaped signal with different time-shaping contrast.

In current high-energy laser experiments, rising edges in the order of several hundred picoseconds are generally required [27]. The fast response time also affects the rising edge speed and shaping ability. Theoretically, OPA has the advantage of a short response time. We simulated fast-rising-edge low-coherence pulse shaping as shown in Figure 3, where the rising edge of the pump was 100 ps and the rising edge of the shaped signal was 65 ps. This demonstrates that our system has the advantage of a faster rising edge and can obtain a rising edge with a magnitude of picoseconds, which satisfies current ICF experimental requirements. According to the OPA principle, the response time of the rising edge of the shaped signal light is related to the response time of the nonlinear process, which can be as short as a few femtoseconds, and the rising time of the pump light. The rising time of the pump light is only limited by conditions that are considerably larger than the response time of the parametric process.

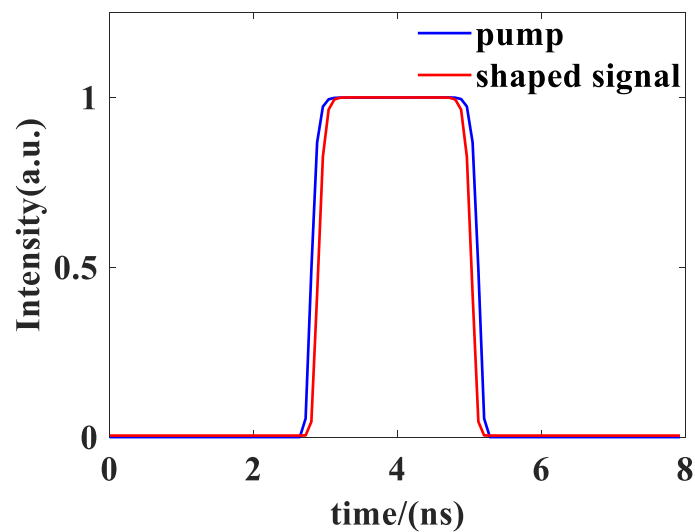


**Figure 3.** Pump pulse and shaped signal pulse with fast rising edge.

Meanwhile, the signal-to-noise ratio is important in arbitrary time shaping and is required to be approximately 40 dB within a few nanoseconds before the pulse [14]. Our OPA-based time-shaping scheme provides a high signal gain owing to its inherent properties and thus has a higher signal-to-noise ratio than other schemes, such as saturable absorption effects [17]. We demonstrated a shaped signal generated with a pump intensity of  $2.5 \text{ GW/cm}^2$  and a signal intensity of  $1 \text{ W/cm}^2$ , as shown in Figure 4. There was a signal-to-noise ratio of over  $10^8$ , which continued to improve as the pump intensity increased in the unsaturated case. This demonstrated that the proposed solution has the advantage of a high signal-to-noise ratio.

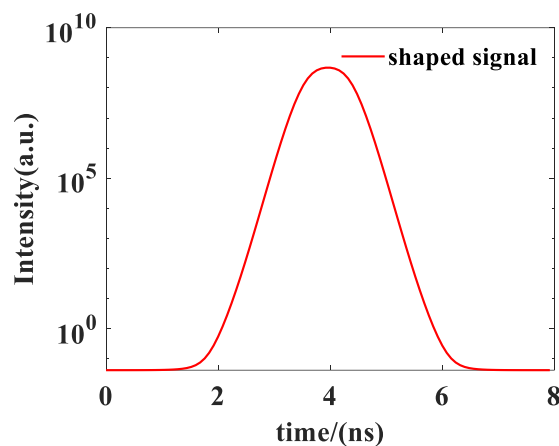


**Figure 4.** Signal-to-noise ratio of the shaped signal.

In addition, the diverse physical requirements of high-energy laser physics experiments require our solution to achieve various waveform outputs such as short pulses [28], short pulse trains, and square waves. We simulated the shaped output signal under the pump using a single short pulse, a short pulse sequence, and the waveforms used in ICF experiments [29], as shown in Figure 5. Pulses shorter than 100 ps, periodic pulses, and arbitrary pulse combinations were obtained. The shaped signal was consistent with the pump waveform (Figure 5). This shows that our scheme can theoretically shape the output of various waveforms accurately to satisfy the requirements of various high-power laser physics experiments. This provides a new shaping scheme for subsequent applications.

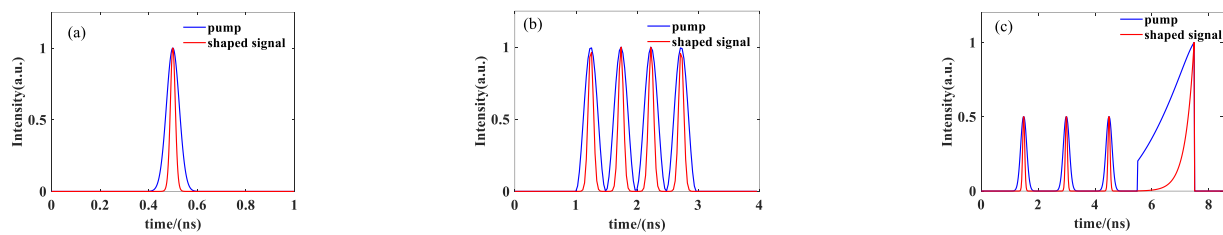


**Figure 5.** Simulation of a wide range of time waveform shaping: (a) short pulse, (b) short pulse trains, and (c) pulse strings required in ICF experiments.

Corresponding to the temporal shaping process described above, the spectral characteristics of the seed source are preserved owing to the physical principle of OPA, which does not result in spectral loss or high-frequency modulation. An advantage of the OPA-based time-shaping scheme is that it ensures a wide spectrum. We simulated broadband light with a central wavelength of 1050 nm and a spectral bandwidth of over 20 nm for shaping and obtained a shaped signal spectrum that maintained broad-spectrum characteristics, as shown in Figure 6. The spectra of the shaped pulses retained their low-coherence characteristics.

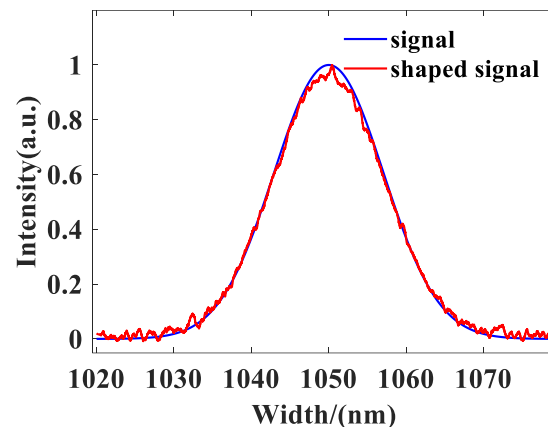


**Figure 6.** Spectral simulation of a broadband signal before and after shaping.

### 3.2. Experimental Arrangement and Results

We built an arbitrary time-shaping system for low-coherence light based on OPA (Figure 7). It primarily consisted of a pump system, a broadband low-coherence light source, and an OPA structure. The pump used an arbitrary time-shaping front end, amplification, and a harmonic conversion scheme commonly used in ICF devices. A distributed-feedback laser was used to produce a continuous 1064 nm narrow-linewidth laser, which was electro-optically modulated and combined with an arbitrary waveform generator (AWG) scheme to achieve arbitrary time shaping. It was then amplified by the fiber amplifier and injected into a solid-state amplifier to increase the energy to 500 mJ, followed by frequency doubling to obtain a 532 nm pump light incident on an LBO crystal with an intensity of approximately  $1 \text{ GW/cm}^2$ . The pump and signal were irradiated together on the LBO crystal to produce OPA interactions with a phase-matched angle. To increase the energy conversion efficiency, we made the pump and signal incident on the crystal at a phase-matching angle. The pump and signal interact at a distance of 25 mm. The pump photons were converted to broad-spectrum signal photons of the corresponding frequency, and the response was time-domain modulated to output a broadband, low-coherence light, time-shaping pulse. The pump shape could be adjusted using an AWG at the front end. The pump energy was controlled by adjusting the gain of the solid-state amplifier. In the proposed scheme, the temporal waveform and spectral characteristics of the shaped output signal were analyzed using an oscilloscope (KEYSIGHT, 4 GHz), a PIN detector (Thorlabs, 5 GHz), and a spectrometer (AvaSpec-Mini4096CL, 0.14 nm). This included analyzing the

temporal waveform correspondence between the output-shaped signal and pump, the shaping capability, and changes in spectral characteristics.

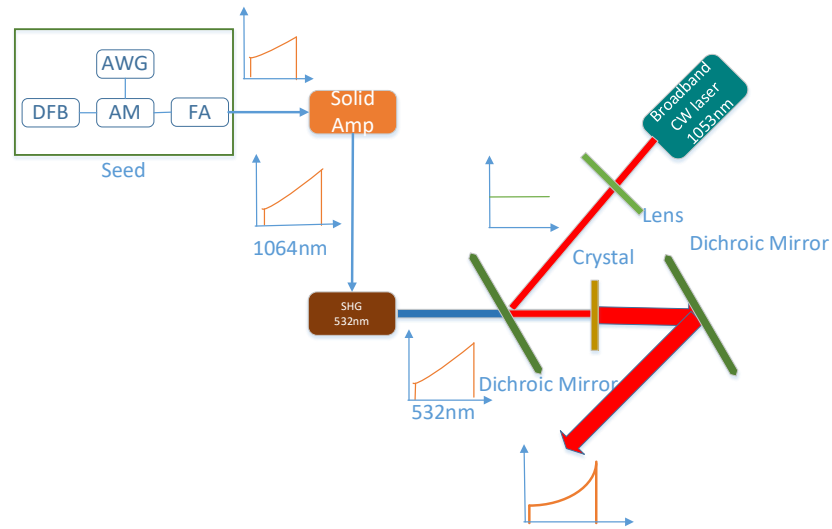


**Figure 7.** Low-coherent light arbitrary time-shaping system based on OPA structure. It primarily consisted of a pump light system, a broadband low-coherence light source, and an OPA structure.

To verify the shaping capability of our arbitrary time-shaping scheme based on the OPA, we injected pump pulses of different time waveform contrasts into the system and observed the time-shaping contrast of the shaped pulses. We used an AWG to generate 1064 nm seed pulses with different time waveform contrasts. The seed pulses were amplified using a solid amplifier and then passed through the frequency doubling system to output a pump pulse of 532 nm. The time waveform contrast of the pump pulse was from 2:1 to 100:1, and an oscilloscope and PIN detector were used to measure the pump after attenuation (Figure 8a) and the shaped signal time profile (Figure 8b). The shaped signal responded well to the intensity waveform of the pump. The signal could be shaped by adjusting the pump waveform. The OPA-based time-shaping scheme presents a significantly higher time-shaping contrast and can exceed the maximum pulse time-shaping contrast of 300:1 within the measurement accuracy range compared with other schemes, such as the 17:1 achievable with saturable absorbers [17]. The experiments showed that the time-shaping contrast of the shaped signal pulse can be controlled by changing the intensity and time waveform contrast of the pump, illustrating the flexibility and controllability of the OPA-based time-shaping scheme in ASE broadband arbitrary time shaping.

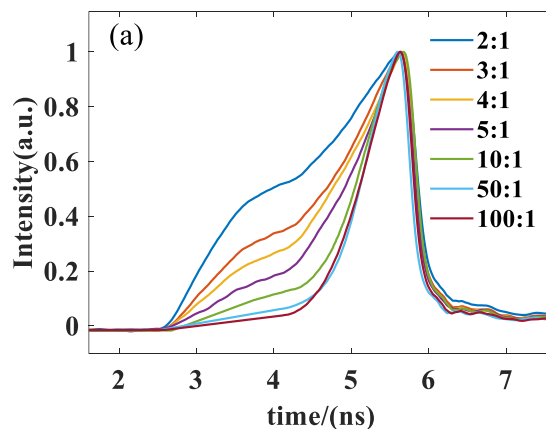


**Figure 8.** Cont.

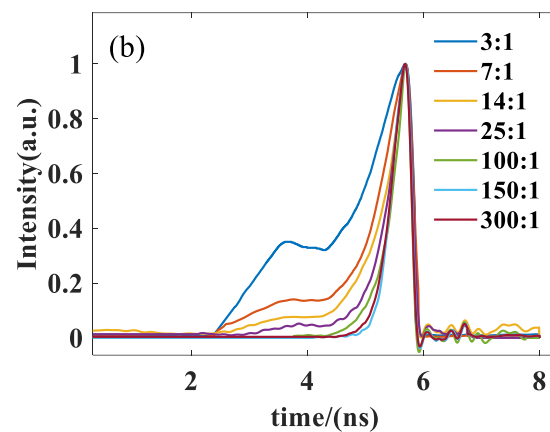


**Figure 8.** Experimental results for (a) the pump with a time waveform contrast from 2:1 to 100:1 and (b) the shaped signal.

The traditional EOM time-shaping scheme is an M-Z interferometer, which may cause time-domain variations in the pulse waveform and introduce high-frequency modulation, which can threaten the safety of high-power physics experimental systems and reduce their output capability [30]. To demonstrate that the OPA-based time-shaping scheme can achieve a smooth time waveform, a square pump pulse was used to amplify the broadband low-coherence signal. Additionally, the shaped signal had a peak modulation of 4% (approximately equal to the unshaped initial amplified spontaneous emission source) (Figure 9b), significantly smaller than the 23% for the conventional shaping scheme (Figure 9c) [17]. The experimental results demonstrated the feasibility of OPA for broadband optical time shaping without introducing additional temporal modulation.

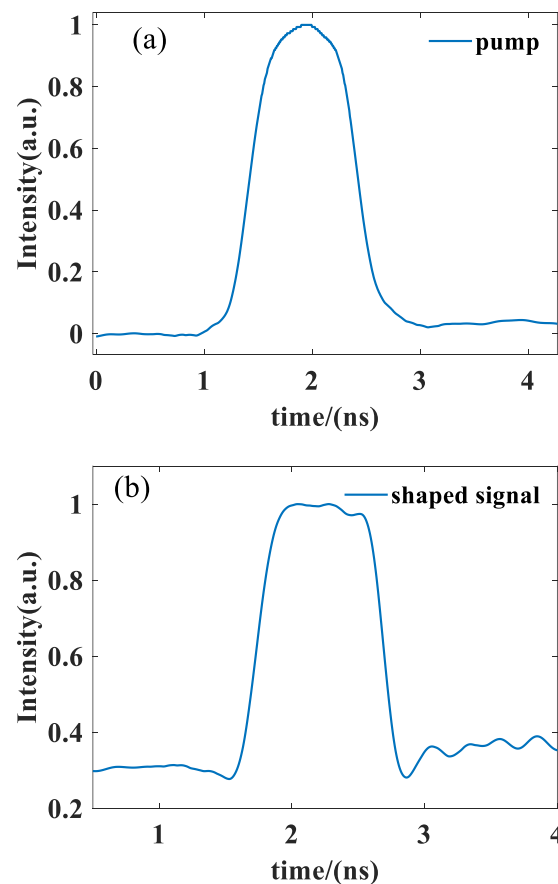


**Figure 9.** Cont.

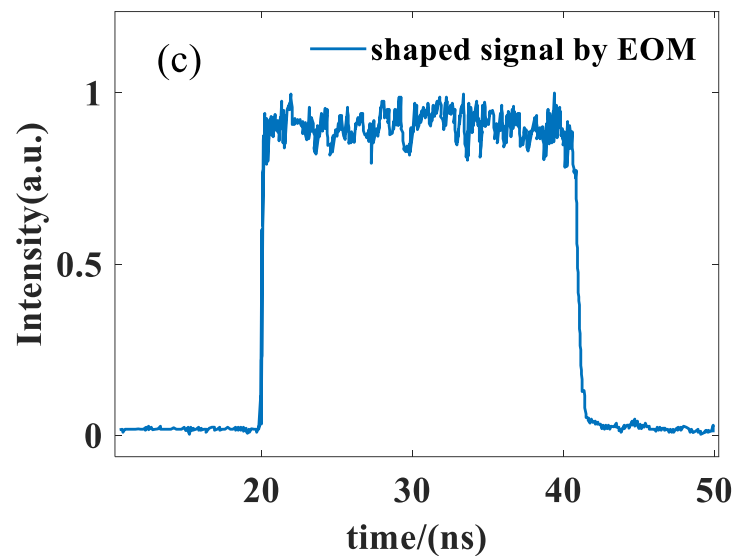


**Figure 9.** Experimental results of OPA-based arbitrary time shaping: (a) time waveform of pump pulse, (b) shaped signal and comparison of the introduced high-frequency modulation based on the (b) OPA-based time-shaping scheme, and (c) conventional shaping scheme.

Additionally, the rise time of the front end of the shaping pulse was extremely short, approximately the same as that of the pump pulse (0.3 ns), indicating that the shaping scheme has the advantage of a short rise time and could achieve a rising edge time on the sub-nanosecond scale. Owing to the energy conservation in the OPA process, the intensity of the output-shaped signal increased with the intensity of the pump and input signals until the optimum input signal and pump energy were reached.

In high-power laser physics experiments, various arbitrary shapes are often required; therefore, adaptation to various physical requirements is also an indication of shaping capability. We obtained a short-pulse pump of 200 ps by adjusting the AWG and shaping a signal pulse with a pulse width of 180 ps (Figure 10a). The pump shape was adjusted to a comb pulse with a period of 200 ps. We obtained a comb-shaped signal pulse with a period of 200 ps (Figure 10b). It responded exactly to the shape of the pump. This demonstrated that the proposed scheme can be adapted to a wide range of physical waveforms.

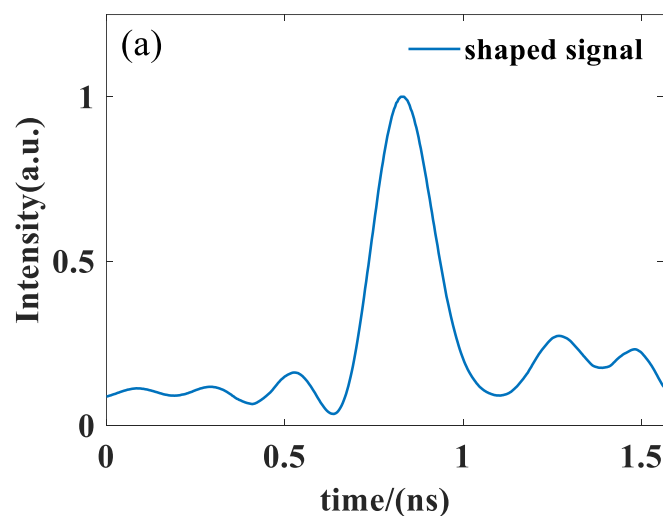


**Figure 10.** Cont.

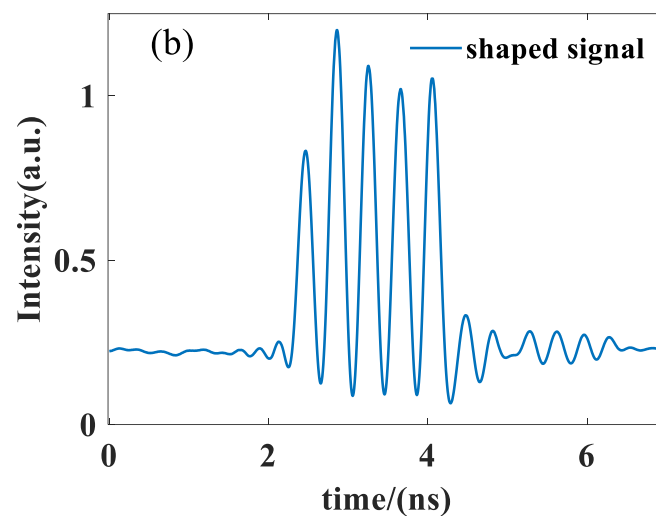


**Figure 10.** Results of various pulse-shaping experiments: (a) short pulse and (b) short pulse train.

The maintenance of the broad-spectral properties of the shaping pulse is important in the broadband low-coherence light time-shaping process. A spectroscopy was used to measure the spectrum. In Figure 11, the blue line shows the spectrum of the pulse passing through the optical path from the ASE source, and the red line shows the spectrum of the shaped and amplified pulse. The spectrum of the shaping pulse remained broad compared with the incident ASE spectrum, with no significant missing spectra, and the spectral width was  $\sim 40$  nm. The experiments demonstrated the broad-spectrum output capability of the proposed scheme.

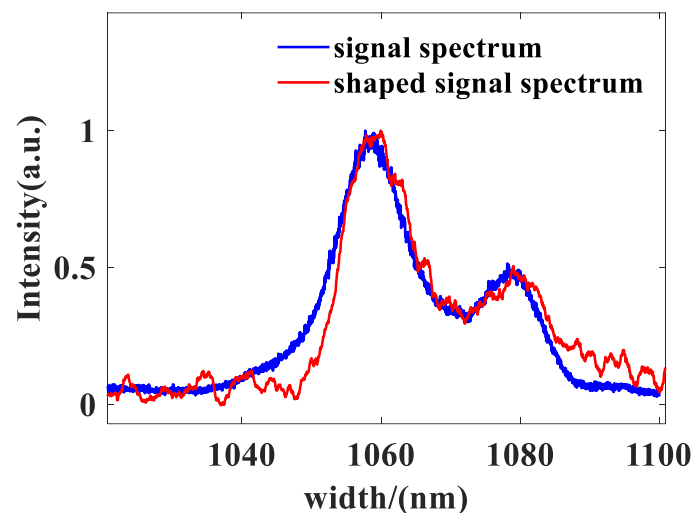


**Figure 11.** Comparison of spectrum in the OPA-based time-shaping experiment. The blue line is the original signal, and the red line is the time-shaped pulse.

From the results in the time and frequency domains, we confirmed the feasibility of our OPA-based time-shaping system for broadband low-coherence optical time-domain shaping.

#### 4. Conclusions

In this study, we analyzed the effect of conventional time shaping on broadband low-coherence light and proposed an OPA-based arbitrary time-shaping scheme for broadband low-coherence light, demonstrating that the OPA can be used for the time shaping of broadband light, and the broadband spectrum characteristics of the shaped pulses can be maintained. We analyzed in detail the variation in the time–frequency characteristics during

broadband low-coherence optical shaping. Compared with conventional shaping schemes, our scheme achieved flexible arbitrary time-shaping capabilities, while missing spectra were significantly reduced and broadband spectrum characteristics were maintained. A higher time-shaping contrast of up to 300:1 or more, fast-rising edges of several hundred picoseconds, and top modulation down to 4% were also obtained. This plays an important role in shaping and applying broadband low-coherence light.

The results of this study demonstrate that this scheme can meet the requirements of the arbitrary time shaping of a high-power laser driver. Due to the current experimental conditions in our lab, the output energy is several nanojoules, which is close to the output capacity of traditional ICF front-end systems. In the next step, using a higher input power will result in a pulse energy of millijoules, which corresponds to the pre-amplifier output energy in the ICF laser driver. Additionally, the output light can be used as the injection pulse with broadband spectra and arbitrary time-shaping abilities to seed the subsequent multi-stage laser amplifiers. More detailed characteristics, including stability, reliability, and control accuracy, need to be studied.

**Author Contributions:** Conceptualization, Y.W. and X.W.; methodology, M.S., X.L. and H.W.; software, M.S.; validation, Y.W. and X.W.; formal analysis, Y.W. and X.W.; investigation, Y.W.; resources, W.F. and X.W.; data curation, X.W. and W.F.; writing—original draft preparation, Y.W.; writing—review and editing, Y.W.; visualization, X.W.; supervision, X.W.; project administration, W.F. and X.W.; funding acquisition, W.F. and X.W. All authors have read and agreed to the published version of the manuscript.

**Funding:** This work was supported by the Strategic Priority Research Program of the Chinese Academy of Sciences (Grant No. XDA25020303).

**Data Availability Statement:** The data included in this study are all owned by the research group and cannot be transmitted.

**Conflicts of Interest:** The authors declare no conflict of interest.

## References

1. Betti, R.; Hurricane, O.A. Inertial-confinement fusion with lasers. *Nat. Phys.* **2016**, *12*, 435–448. [[CrossRef](#)]
2. Labaune, C. Incoherent light on the road to ignition. *Nat. Phys.* **2007**, *3*, 680–682. [[CrossRef](#)]
3. Montgomery, D.S. Two decades of progress in understanding and control of laser plasma instabilities in indirect drive inertial fusion. *Phys. Plasmas* **2016**, *23*, 055601. [[CrossRef](#)]
4. Kato, Y.; Mima, K.; Miyanaga, N.; Arinaga, S.; Kitagawa, Y.; Nakatsuka, M.; Yamanaka, C. Random Phasing of High-Power Lasers for Uniform Target Acceleration and Plasma-Instability Suppression. *Phys. Rev. Lett.* **1984**, *53*, 1057–1060. [[CrossRef](#)]
5. Skupsky, S.; Short, R.W.; Kessler, T.; Craxton, R.S.; Letzring, S.; Soures, J.M. Improved laser-beam uniformity using the angular dispersion of frequency-modulated light. *J. Appl. Phys.* **1989**, *66*, 3456–3462. [[CrossRef](#)]
6. Arefiev, A.; Gong, Z.; Robinson, A.P.L. Energy gain by laser-accelerated electrons in a strong magnetic field. *Phys. Rev. E* **2020**, *101*, 043201. [[CrossRef](#)]
7. Hussein, A.E.; Arefiev, A.V.; Batson, T.; Chen, H.; Craxton, R.S.; Davies, A.S.; Froula, D.H.; Gong, Z.; Haberberger, D.; Ma, Y.; et al. Towards the Optimisation of Direct Laser Acceleration. *J. Phys.* **2021**, *23*, 023031. [[CrossRef](#)]
8. Nakano, H.; Kanabe, T.; Yagi, K.; Tsubakimoto, K.; Nakatsuka, M.; Nakai, S. Amplification and propagation of partially coherent amplified spontaneous emission from Nd-glass. *Opt. Commun.* **1990**, *78*, 123–127. [[CrossRef](#)]
9. Nakano, H.; Tsubakimoto, K.; Miyanaga, N.; Nakatsuka, M.; Kanabe, T.; Azechi, H.; Jitsuno, T.; Nakai, S. Spectrally dispersed amplified spontaneous emission for improving irradiation uniformity into high-power Nd-glass laser system. *J. Appl. Phys.* **1993**, *73*, 2122–2131. [[CrossRef](#)]
10. Nakano, H.; Miyanaga, N.; Yagi, K.; Tsubakimoto, K.; Kanabe, T.; Nakatsuka, M.; Nakai, S. Partially coherent light generated by using single and multimode optical fibers in a high-power Nd-glass laser system. *Appl. Phys. Lett.* **1993**, *63*, 580–582. [[CrossRef](#)]
11. Cui, Y.; Gao, Y.; Rao, D.; Liu, D.; Li, F.; Ji, L.; Shi, H.; Liu, J.; Zhao, X.; Feng, W.; et al. High-energy low-temporal-coherence instantaneous broadband pulse system. *Opt. Lett.* **2019**, *44*, 2859–2862. [[CrossRef](#)]
12. Li, F.; Gao, Y.; Ji, L.; He, R.; Liu, D.; Zhao, X.; Xia, L.; Feng, L.; Shi, H.; Rao, D.; et al. Characteristics of the beam smoothing using the combination of induced spatial incoherence and continuous phase plate. *Opt. Laser Technol.* **2022**, *145*, 107537. [[CrossRef](#)]
13. Dorrer, C.; Hill, E.M.; Zuegel, J.D. High-energy parametric amplification of spectrally incoherent broadband pulses. *Opt. Express* **2020**, *28*, 451–471. [[CrossRef](#)] [[PubMed](#)]
14. Fan, W.; Jiang, Y.; Wang, J.; Wang, X.; Huang, D.; Lu, X.; Wei, H.; Li, G.; Pan, X.; Qiao, Z.; et al. Progress of the injection laser system of SG-II. *High Power Laser Sci. Eng.* **2018**, *6*, e34. [[CrossRef](#)]

15. Browning, D.F.; Rothenberg, J.E.; Wilcox, R.B. The issue of FM to AM conversion on the National Ignition Facility. In Proceedings of the Third International Conference on Solid State Lasers for Application to Inertial Confinement Fusion, Pts 1 and 2, Monterey, CA, USA, 7–12 June 1998; Volume 3492, pp. 51–61.
16. Bouyer, C.; Parreault, R.; Roquin, N.; Natoli, J.-Y.; Lamaignère, L. Impact of temporal modulations on laser-induced damage of fused silica at 351 nm. *High Power Laser Sci. Eng.* **2023**, *11*, e5. [[CrossRef](#)]
17. Sui, D.; Li, R.; Sun, M.; Wang, X. All-optical arbitrary temporal shaping technology of broadband low-coherence light based on saturable absorption effect. In Proceedings of the Volume 11181, High-Power Lasers and Applications X, Hangzhou, China, 19 November 2019; Volume 111810, pp. 47–55.
18. Dorrer, C.; Spilatro, M. Spectral and temporal shaping of spectrally incoherent pulses in the infrared and ultraviolet. *Opt. Express* **2022**, *30*, 4942–4953. [[CrossRef](#)]
19. Devaux, F.; Lantz, E. Parametric amplification of a polychromatic image. *Optica* **1995**, *12*, 2245–2252. [[CrossRef](#)]
20. Manzoni, C.; Cirmi, G.; Brida, D.; De Silvestri, S.; Cerullo, G. Optical-parametric-generation process driven by femto-second pulses: Timing and carrier-envelope phase properties. *Phys. Rev.* **2009**, *73*, 033818. [[CrossRef](#)]
21. Picozzi, A.; Montes, C.; Haelterman, M. Coherence properties of the parametric three-wave interaction driven from an incoherent pump. *Phys. Rev. E* **2002**, *66*, 056605. [[CrossRef](#)]
22. Thomson, J.J.; Karush, J.I. Effects of finite-bandwidth driver on parametric-instability. *Phys. Fluids* **1974**, *17*, 1608–1613. [[CrossRef](#)]
23. Obenschain, S.P.; Luhmann, J.N.C.; Greiling, P.T. Effects of Finite-Bandwidth Driver Pumps on Parametric-Decay Instability. *Phys. Rev. Lett.* **1976**, *36*, 1309–1312. [[CrossRef](#)]
24. Palastro, J.P.; Shaw, J.G.; Follett, R.K.; Colaitis, A.; Turnbull, D.; Maximov, A.V.; Goncharov, V.N.; Froula, D.H. Resonance absorption of a broadband laser pulse. *Phys. Plasmas* **2018**, *25*, 123104. [[CrossRef](#)]
25. Arisholm, G. Quantum noise initiation and macroscopic fluctuations in optical parametric oscillators. *Optica* **1999**, *16*, 117–127. [[CrossRef](#)]
26. Milonni, P.W.; Auerbach, J.; Eimerl, D. Frequency conversion modeling with spatially and temporally varying beams. In Proceedings of the 1st Annual International Conference on Solid State Lasers for Application to Inertial Confinement Fusion, Monterey, CA, USA, 8 December 1995.
27. Zhu, J.; Zhu, J.; Li, X.; Zhu, B.; Ma, W.; Lu, X.; Fan, W.; Liu, Z.; Zhou, S.; Xu, G.; et al. Status and development of high-power laser facilities at the NLHPLP. *High Power Laser Sci. Eng.* **2018**, *6*, e55. [[CrossRef](#)]
28. Roeder, S.; Zobus, Y.; Brabetz, C.; Bagnoud, V. How the laser beam size conditions the temporal contrast in pulse stretchers of chirped-pulse amplification lasers. *High Power Laser Sci. Eng.* **2022**, *10*, e34. [[CrossRef](#)]
29. Zou, L.; Geng, Y.; Liu, B.; Chen, F.; Zhou, W.; Peng, Z.; Hu, D.; Yuan, Q.; Liu, G.; Liu, L. CNN-based neural network model for amplified laser pulse temporal shape prediction with dynamic requirement in high-power laser facility. *Opt. Express* **2022**, *30*, 29885–29899. [[CrossRef](#)] [[PubMed](#)]
30. Zuo, J.X.; Lin, X.C. High-Power Laser Systems. *Laser Photonics Rev.* **2022**, *16*, 2100741. [[CrossRef](#)]

**Disclaimer/Publisher’s Note:** The statements, opinions and data contained in all publications are solely those of the individual author(s) and contributor(s) and not of MDPI and/or the editor(s). MDPI and/or the editor(s) disclaim responsibility for any injury to people or property resulting from any ideas, methods, instructions or products referred to in the content.